JGR Atmospheres

RESEARCH ARTICLE
10.1029/2020JD033818

Spatiotemporal Variability of the Southern Annular Mode and its Influence on Antarctic Surface Temperatures

Paul Wachter[1], Christoph Beck[2], Andreas Philipp[2], Kathrin Höppner[3], and Jucundus Jacobeit[2]

[1]German Remote Sensing Data Center (DFD), German Aerospace Center (DLR), Wessling, Germany, [2]Institute of Geography, Augsburg University, Augsburg, Germany, [3]Institute Development-Space Research and Technology (VO-IR), German Aerospace Center (DLR), Köln, Germany

Key Points:
- We present a new approach to examine the spatiotemporal Southern Annular Mode pattern variability
- Station-based Antarctic temperature anomalies are related to different structures of the Southern Annular Mode
- The trend pattern shows an increasing meridional structure and correlations with Pacific and Atlantic multidecadal oscillations

Correspondence to:
P. Wachter,
paul.wachter@dlr.de

Citation:
Wachter, P., Beck, C., Philipp, A., Höppner, K., & Jacobeit, J. (2020). Spatiotemporal variability of the Southern Annular Mode and its influence on Antarctic surface temperatures. *Journal of Geophysical Research: Atmospheres*, *125*, e2020JD033818. https://doi.org/10.1029/2020JD033818

Received 1 SEP 2020
Accepted 12 NOV 2020
Accepted article online 21 NOV 2020

Abstract The Southern Annular Mode (SAM) is the predominant atmospheric variability mode in the Southern Hemisphere. In this paper, we present the spatial variability results of the SAM pattern for the period 1979–2018. The SAM-intrinsic pattern variability analysis is based on the principal component analysis (PCA), which is carried out for the ERA-Interim 500 hPa geopotential height (GPH) data set. A spatiotemporally resolved data set of SAM pattern maps (PCA loadings) is derived by projecting monthly shifted sub-sequences of SAM index values (PCA scores) on the corresponding GPH anomalies. The dominant SAM structure within single pattern fields is mapped automatically and can be interpreted as the Southern Hemisphere polar front. This data set allows an analysis of the geographical positions of the characteristic circumpolar SAM structure over four decades and shows considerable variability over space and time. Five different states of SAM patterns, which are associated with characteristic circulation anomalies during different phases of the study period, are identified. Station-based Antarctic temperature anomalies can be synoptically explained by these circulation anomalies. The overall latitudinal trend of the SAM pattern indicates an intensification of the meridional structure, especially over the East Antarctic Southern Ocean. Furthermore, we show that the SAM pattern variability is significantly correlated with the Pacific Decadal Oscillation and the Atlantic Multidecadal Oscillation. Composites of 500 hPa GPH anomalies during the positive and negative phases of the respective indices indicate teleconnections with Pacific Decadal Oscillation and Atlantic Multidecadal Oscillation, and this can explain latitudinal trends of the SAM pattern.

1. Introduction

The Southern Annular Mode (SAM), also known as the Antarctic Oscillation, is the dominant atmospheric circulation variability mode in the Southern Hemisphere (SH) (Thompson & Wallace, 2000). In this study, we use the term SAM even if the cited literature uses Antarctic Oscillation because both parameters represent the same pattern of SH circulation variability. The SAM index is a time series, which describes the month-to-month variability in the SH extratropical circulation between the low pressure located over polar latitudes and the relatively high pressure at midlatitudes. The positive (negative) polarity of SAM is interpreted as a condition of increased (reduced) pressure gradient between midlatitudes and polar latitudes (Gong & Wang, 1999; Marshall et al., 2006; Thompson & Wallace, 2000). Thus, the SAM also indicates the strength of the SH circumpolar flow (Jones et al., 2009). The SAM can be calculated in three different ways. Gong and Wang (1999) calculated the SAM as the normalized pressure gradient between 40°S and 65°S from gridded data sets. Thompson and Wallace (2000) used principal component analysis (PCA) of gridded mean sea level pressure (MSLP) and geopotential height (GPH) fields, and they defined the leading principal component (first principal component) as the SAM. An observation-based approach for deriving the SAM is provided by Marshall (2003). He used pressure data from stations along the Antarctic coast and selected midlatitude stations. Additional information about the different methods used to calculate the SAM and a comparison of different SAM time series was given by Jones et al. (2009), Ho et al. (2012), and Fogt and Marshall (2020). Especially Fogt and Marshall (2020) provide a comprehensive overview over the scientific understanding and the importance of the SAM in SH climate research and motivate further studies on this topic in the future.

Temporal trends in the SH pressure fields and the SAM were described by Marshall (2003, 2007) for the period of 1957–2004 and by Visbeck (2009) for 1970–2005. They found positive trends in the SAM for the austral

summer (December, January, and February [DJF]) and autumn (March, April, and May [MAM]). For the period since 1998, Turner et al. (2016) reported the absence of further temperature increases at the Antarctic Peninsula, which is related to a negative SAM trend during DJF. SAM time series are frequently used to explain variabilities of near-surface geophysical parameters dependent on the large-scale circulation variability. Van den Broeke and van Lipzig (2004) discussed the influences of the SAM on climate variables such as temperature, wind, and precipitation. In their study, a high SAM resulted in warming of the Antarctic Peninsula and cooling over most other parts of the Antarctic continent. Strong circumpolar westerlies mean an intensified advection of oceanic air toward the Antarctic Peninsula, which leads to above-average temperatures. In other, more continental regions of Antarctica, such as East Antarctica and the plateau, a positive SAM leads to reduced meridional air flow resulting in a cooling pattern (Kwok & Comiso, 2002; Thompson & Solomon, 2002; Van den Broeke & van Lipzig, 2004).

SAM trends are known to be related to stratospheric ozone depletion during the austral spring (September, October, and November [SON]) (Arblaster & Meehl, 2006). According to Thompson et al. (2011), the increased SH meridional temperature gradient observed in the stratosphere due to reduced ultraviolet radiation absorption during the ozone hole season leads to an acceleration of the stratospheric polar vortex. As a result of dynamical coupling from the stratosphere to the troposphere, the signature of this stratospheric circulation intensification can also be found in the tropospheric SAM (Previdi & Polvani, 2014). In their study, Previdi and Polvani (2014) described a poleward shift of the troposphere jet and the midlatitude westerly winds as a circulation-dynamical result of the thermal influence of the ozone hole. Shindell and Schmidt (2004) studied the relative influence of ozone depletion and the increase in the amount of greenhouse gases in the SH. With their modeling approach, they were able to show that the influence of the ozone hole dominated the positive SAM trend over the past decades (see also Arblaster & Meehl, 2006, and references therein).

Tropospheric factors influencing the Antarctic climate are related to teleconnections from the tropical Pacific. The Pacific-South American (PSA) mode describes a Rossby wave train pattern between the tropical western Pacific and the South American region (Ding et al., 2012). The influence of this mode induces a strong zonally asymmetric component in the West Antarctic region, whereas the East Antarctic sector (0–180°) is characterized by a distinct zonal SAM pattern (Ding et al., 2012; Fogt, Jones, et al., 2012). Marshall and Thompson (2016) examined the influence on Antarctic surface air temperatures for four different variability modes. They were able to show that the SAM has a significant influence on Antarctic temperatures on the entire continent throughout the year. Furthermore, they found that the patterns PSA1 and PSA2 have a higher regional influence in the western hemisphere than SAM, except during the SH summer season. As shown by Clem, Renwick, and McGregor (2016), SAM trends in the Pacific region are significant in DJF and MAM, whereas positive trends in the Indian Ocean sector are only found during DJF. For the entire hemisphere, they found positive trends during both DJF and MAM (Clem, Renwick, & McGregor, 2016). Furthermore, Clem, Renwick, McGregor, and Fogt (2016) provided an estimate of the seasonally varying influence of the SAM and the Southern Oscillation on the temperature variability of the Antarctic Peninsula. The Southern Oscillation has its highest influence on West Antarctic temperatures in austral winter (June, July, and August [JJA]) and SON. Nicolas et al. (2017) demonstrated the high potential of the Southern Oscillation in the Pacific Basin to cause an exceptional warming and melting event in the West Antarctic region in January 2016. This warming and surface melting in the West Antarctic was also reported by Scott et al. (2019), and it is favored by an intense Amundsen Sea low during negative SAM phases. A strong El Niño-Southern Oscillation (ENSO) teleconnection pattern over the West Antarctic is also known for La Niña cases in combination with positive SAM phases and for El Niño events in combination with negative SAM conditions (Fogt et al., 2011). On longer, multiannual to multidecadal time scales, the influence of Pacific and Atlantic sea surface temperatures (SSTs) modulates the Antarctic circumpolar circulation and regional Antarctic climate. Motivated by Zhang et al. (1996), Garreaud and Battisti (1999) examined decadal ENSO-like signatures in extratropical SH circulation variability. They described that decadal ENSO-like variability favors a circum-Antarctic zonal wavenumber three anomaly pattern along 60°S. This tropical forcing mechanism was also investigated by Clem and Fogt (2015), who found a Rossby wave train from the tropical Pacific toward the Ross Sea driven by the Pacific Decadal Oscillation (PDO). In addition to the Pacific teleconnection patterns, Li et al. (2014) showed that Rossby wave trains, originating in the tropical and northern Atlantic, influence sea ice and temperature around the Antarctic continent

(see also Li et al., 2015). They linked this Atlantic-Antarctic teleconnection to changes in the Atlantic Multidecadal Oscillation (AMO). Kayano and Setzer (2018) also found a multidecadal relation between AMO-induced circulation anomalies and temperature variations in Punta Arenas, southern Chile.

The literature cited above provides an overview of the spatial and temporal scales on which circulation variabilities can affect the Antarctic climate. In this study, we investigated the spatiotemporal variability patterns of the SAM in more detail. Seasonal zonal asymmetries of the SAM pattern have been described by Fogt, Jones, et al., (2012), whereas we focus on spatial variations on multiannual to decadal time scales. In section 2, we provide an overview of the data sets employed and new methodologies applied to compare different SAM time series and derive spatiotemporally resolved SAM pattern data. The results of the spatiotemporal variability of the SAM structure are presented in section 3, which are mainly based on the annularity of the SAM pattern. Our analysis allows for the first time a presentation of the spatiotemporal variability of the SAM pattern that is oriented on its prevailing circumpolar structure. It is our aim to provide a holistic view of the essential spatiotemporal properties of this dominant circulation mode of the SH by using Hovmöller diagrams. With this approach, we visualize variabilities and changes in the SAM pattern in a more illustrative way. In particular, we can directly assess the annularity of the SAM pattern, whose spatiotemporal variability shows large variations over the past four decades. Based on these initial results, we identified five dominant SAM structures which occur during different periods of the study period. Atmospheric circulation composites of the five different clusters were interpreted with respect to their influence on Antarctic surface temperatures. Furthermore, we analyzed significant spatial trends, which we interpreted as long-term shifts of the SAM structure. These changes in the dominant circulation pattern of the SH were related to the influence of long-term changes in PDO and AMO.

2. Data and Methods

2.1. Data Employed

In this study, we used three different reanalysis data sets to derive SAM time series and compare them with frequently used and freely available SAM time series. The following list provides an overview of these data sets and their references:

1. ERA-Interim reanalysis, European Centre for Medium-Range Weather Forecasts, Dee et al. (2011).
2. National Centers for Environmental Predictions (NCEP)/National Center for Atmospheric Research (NCAR) reanalysis, Kalnay et al. (1996).
3. JRA-55 reanalysis, Japanese 55-year Reanalysis, Japan Meteorological Agency, Kobayashi et al. (2015).
4. SAM by National Oceanic and Atmospheric Administration (NOAA)/Climate Prediction Center (CPC), CPC of the NOAA.
5. SAM by G. Marshall, British Antarctic Survey, Marshall (2003).

Monthly averaged GPH data of the 500 hPa level, at a spatial resolution of 2.5° × 2.5°, south of 30°S, were used to derive the SAM time series for the period 1979–2018. Since SAM analyses are usually based on anomaly data, the long-term seasonal signal of the GPH data was removed. For this study, we used the 30 year reference period, 1981–2010, to calculate the monthly anomaly data. With respect to the meridian convergence and to avoid overestimation of the influence of high polar latitudes, the data fields were weighted by the square root of the cosine according to their geographic latitudes. In section 3.2., we additionally used monthly ERA-Interim 10 m u- and v-wind data at a resolution of 0.5° × 0.5°. The wind anomaly composites employed also refer to the 1981–2010 reference period. The SAM time series from NOAA/CPC and Marshall were not edited or manipulated because they were used as reference data sets for comparison with our PCA-based SAM analysis of the three different reanalysis data sets.

Antarctic station temperature data were taken from the CRUTEM4 data set, Version 4.6.0.0 (Jones et al., 2012). Their data set provides a quality-controlled and regularly updated database for the analysis of monthly aggregated temperature observations around Antarctica. As not all Antarctic stations cover the entire study period and data from some contain significant gaps, we only used time series of stations that contain at least 90% valid data records of the study period from 1979 to 2018. Temperature anomalies were derived by subtracting long-term monthly mean values of the reference period 1981–2010 to ensure consistency with the procedure applied for GPH anomaly fields. Figure 1 gives an overview of the Antarctic

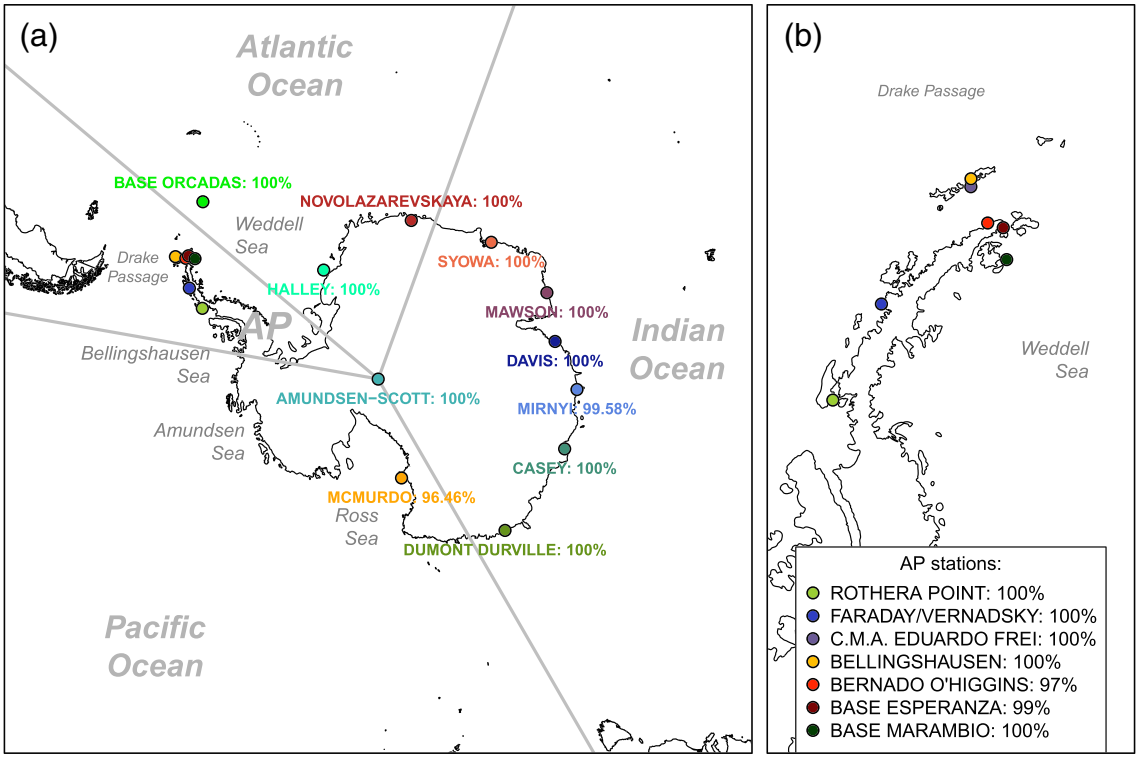

Figure 1. (a) Overview map of Antarctic stations and their percentages of valid monthly data records from January 1979 to December 2018 as they are provided by the CRUTEM4 data set; and (b) regional map for Antarctic Peninsula stations.

stations and their percentage of valid temperature data records. The map contains the names of geographic regions as they are referred to in this paper.

In addition to the SAM index time series from the above-mentioned sources, we employed ocean-related variability indices to investigate their possible teleconnections with SH polar circulation variability. Data of the PDO index were obtained from NOAA's National Centers for Environmental Information (Mantua & Hare, 2002) and the AMO time series from NOAA's Physics Science Laboratory (Enfield et al., 2001).

2.2. SAM Analysis

As mentioned in section 1, there are three different approaches to calculate the SAM index time series. Gong and Wang (1999) defined the SAM index, also called the Antarctic Oscillation Index, as the difference of normalized monthly zonal MSLP data between midlatitudes (40°S) and subpolar (65°S) latitudes:

$$\mathbf{SAM}(\mathbf{t}) = \mathbf{P}^{*}_{\mathbf{40°S}}(\mathbf{t}) - \mathbf{P}^{*}_{\mathbf{65°S}}(\mathbf{t}). \quad (1)$$

They used the gridded NCEP/NCAR reanalysis data set to derive the SAM index, whereas Marshall (2003) carried out the SAM analysis based on six midlatitude stations and six coastal Antarctic stations. Both approaches directly address the annular meridional pressure gradient between midlatitudes and subpolar latitudes, whereas the PCA-based methodology also contains information about the pressure variability at high and lower SH latitudes. In our study, the SAM was derived by applying an unrotated s-mode PCA to obtain a high explained variance for the first principal component. Furthermore, it is necessary to distinguish PCAs based on correlation or covariance matrices. Because the input data of GPH anomalies are measured in the same unit and the variables comprise a homogenous variance range, the use of the covariance matrix is preferred in this study (Wilks, 2005). According to the definition of a reference period (see section 2.1), PCA was applied only for the data period from 1981 to 2010 in order to obtain the principal component-loading pattern. The loading pattern of the first principal component represents the SAM

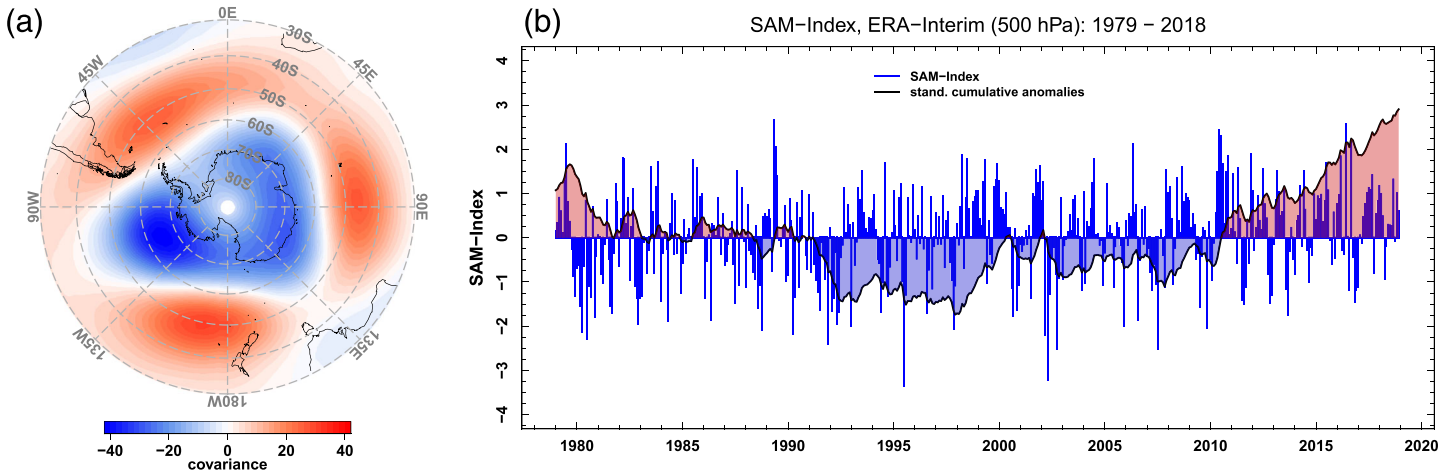

Figure 2. Southern Annular Mode (SAM) analysis of the ERA-Interim 500 hPa level. (a) The SAM pattern represents the leading principal component-loading pattern of the reference period 1981–2010; (b) the SAM index time series is indicated by blue bars, and the cumulative SAM index is represented by the black solid line. This leading principal component explains 23.4% of the SH 500 hPa GPH variability.

pattern appearing with the well-pronounced variability centers between midlatitudes and subpolar latitudes (see Figure 2a; ERA-Interim 500 hPa level). This reference pattern is used to derive the SAM time series of the entire period 1979–2018 by projecting the principal component-loading pattern onto the monthly GPH anomaly data. Hereby, the product of the GPH anomaly field ***GPH**** of a single time unit ***tp*** and the principal component-loading pattern ***PCload*** is summed up over all grid points ***ngp***:

$$SAM^*_{tp} = \sum_{gp=1}^{ngp}\left(GPH^*_{gp,\,tp} \cdot PCload_{gp}\right). \tag{2}$$

The compiled time series SAM^* is standardized relative to the mean $\overline{SAM^*_{ref}}$ and standard deviation $\sqrt{Var\left(SAM^*_{ref}\right)}$ of the reference period:

$$SAM = \frac{SAM^* - \overline{SAM^*_{ref}}}{\sqrt{Var\left(SAM^*_{ref}\right)}}. \tag{3}$$

To highlight long-term changes in the course of the SAM time series, another statistical assessment was applied. The cumulative SAM index value for each time unit $scSAM^*_{tp}$ is calculated according to

$$scSAM^*_{tp} = \sum_{i=1}^{tp} SAM_{tp}. \tag{4}$$

This original time series $scSAM^*$ is also standardized relative to the mean $\overline{scSAM^*}$ and standard deviation $\sqrt{Var(scSAM^*)}$.

Figure 2a shows the spatial pattern of the leading principal component calculated for the reference period 1981–2010 and the SAM index time series (Figure 2b) for the entire period 1979–2018 for the ERA-Interim 500 hPa level. The pattern exhibits the expected feature of opponent pressure variability between midlatitudes and polar latitudes. A distinct and intense center of variability is located in the Amundsen Sea, which describes a zonal anomaly compared with the circumpolar structure parallel to the East Antarctic continent (Fogt, Jones, et al, 2012; Fogt, Wovrosh, et al., 2012; Hosking et al., 2013). The mid-latitude centers of variability are located over the southwest Atlantic Ocean, centered at 90°E over the Indian Ocean and in the southeast Pacific. The interpretation of the SAM index time series (blue bars in Figure 2b)

is limited to certain months or seasons with significant high or low index values. In combination with the cumulative SAM, phases of positive (red shaded) or negative (blue shaded) SAM conditions can be identified. The first years—from 1980 to 1983—show a mainly negative SAM, indicated by a decrease in the cumulative SAM. Another period of negative SAM conditions was found in 1991 and 1992. For the Years 1998–2001, the SAM is predominantly in a positive phase, as is also the case for the period since 2008. For these phases, the curve of the cumulative SAM shows a continuous increase, which indicates an accumulation of positive SAM values.

This commonly accepted and widely used analysis approach was extended to an analysis of the spatiotemporal variability of the SAM pattern. The SAM pattern $\boldsymbol{PCload_{lon,lat}}$ is the regression map (in this study the covariance) of the SAM index time series $\boldsymbol{SAM_{per}}$ and the GPH anomalies $\boldsymbol{GPH^{*}_{lon,\,lat,\,per}}$ for a defined period ***per***, as shown in Figure 2a for the reference period from 1981 to 2010:

$$PCload_{lon,\,lat} = Cov\left(GPH^{*}_{lon,\,lat,\,per}, SAM_{per}\right). \tag{5}$$

By choosing a smaller regression period *per* in Equation 5, a spatiotemporally resolved SAM pattern data set was derived. In this study, the regression window length was 60 months, and it was shifted successively by 1 month. A regression period length of 60 months was chosen to exclude monthly to multiseasonal circulation anomalies related to the ENSO system. In addition, this regression period is short enough to allow investigations of variabilities on multiannual to decadal time scales. To obtain information about the spatiotemporal variability of the SAM pattern (cf. Figure 2a), the transition zone between midlatitudes and subpolar latitudes was mapped with an automated algorithm that identifies the SAM pattern regions of minimum covariance. For this purpose, the latitude with the smallest absolute covariance was determined for each longitude on the lat-lon grid, and thus, a spatiotemporal mapping of the circumpolar SAM structure was achieved. Since this mapping was performed on the 2.5° × 2.5° grid of the ERA interim data set, the SAM structures were smoothed using a spline function for the presentation in Figure 4 (and Appendix A). This transition zone between positive (midlatitudes) and negative (subpolar latitudes) covariance is interpreted as the structure of the SAM pattern and is of specific interest in this study. Its spatiotemporal latitudinal positions reveal considerable variabilities and trends and will be discussed in more detail in section 3.

2.3. SAM Assessment

To ensure that the SAM method and the ERA-Interim data set are consistent with the comparable SAM time series, both SAM and cumulative SAM time series were compared with the SAM data provided by Marshall (2003) and NOAA/CPC. Figure 3a provides a correlation matrix for the PCA-based SAM analysis (see Equations 2 and 3) for the 500 hPa GPH levels of the ERA-Interim, NCEP/NCAR, and JRA-55 data sets, and the SAM time series was provided by the SAM based on 500 hPa GPH gradients between midlatitudes and polar latitudes (Gong & Wang, 1999, Equation 1). In this assessment, we generally found high correlations with significance at $p < 0.001$ in a two-sided t test. The highest correlations for all three PCA-based SAM time series of the reanalysis data sets were found for NOAA/CPC's SAM. Their SAM is also based on PCA, whereas Marshall uses station observations. The other SAM time series represent latitude-based gradients. Larger differences between the data sets and the different methods become apparent when considering the time series of the cumulative SAM. Figure 3b shows that the PCA-based cumulative SAM is moderately correlated with the cumulative SAM of NOAA/CPC and significantly correlated with the latitude-based cumulative SAM of the three reanalysis data sets. Only the PCA-based NCEP/NCAR cumulative SAM shows moderate correlations with the cumulative SAM of NOAA/CPC. The uncorrelated relationship between Marshall's cumulative SAM and the PCA-based cumulative SAM is likely caused by different methodologies (station based vs. PCA) and the data used (MSLP observations vs. 500 hPa GPH reanalysis). The significances in Figure 3a, and especially for the cumulative SAM time series in Figure 3b, were derived by considering the autocorrelation by a reduction of the degrees of freedom when deriving the correlation test statistics.

Due to the temporally integrating approach, the cumulative SAM is sensitive to accumulations of higher or lower values of SAM time series and thus also to trends, whereas the correlation of SAM time series is only a

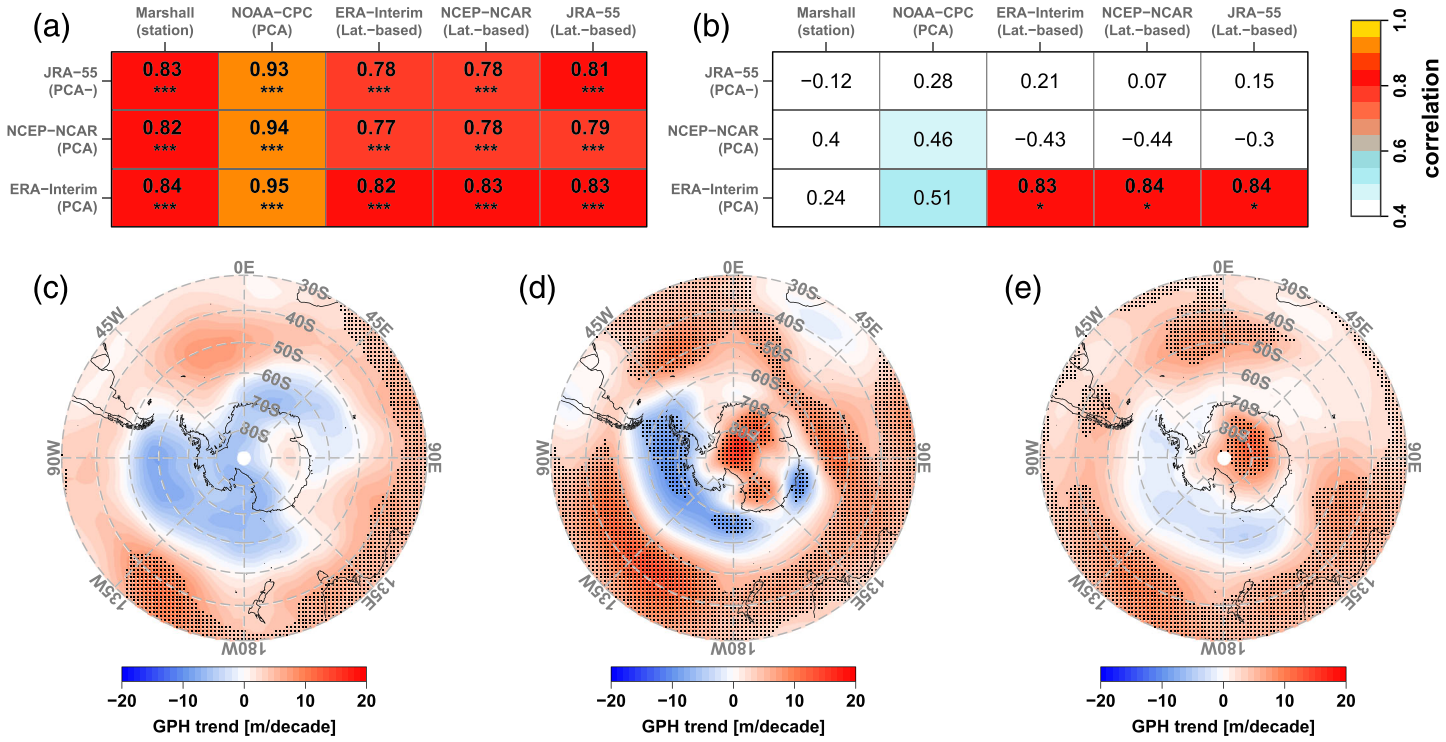

Figure 3. (a) indicates correlation (Spearman) statistics for the principal component analysis (PCA)-based SAM time series of three reanalysis data sets, freely available SAM analysis, and the latitude-based SAM time series as they were derived by Gong and Wang (1999); (b) the same correlation statistics as in (a) were used but for the cumulative SAM of the respective SAM time series; (c–e) 500 hPa GPH trends for (c) ERA-Interim, (d) NCEP/NCAR, and (e) JRA-55. Correlations and trends were calculated for the reference period from January 1981 to December 2010. The significance of correlations is the following: *** $p < 0.001$, ** $p < 0.01$, and * $p < 0.1$. Dotted areas in (c)–(e) indicate the trend significance of the Mann-Kendall test at $p < 0.01$.

measure for the relative relationship between SAM time series. As the correlations of the cumulative SAM in Figure 3b show, there must be differences in the presence of higher or lower SAM values over time between the different approaches and between the three data sets used in this study. As mentioned in section 1 and indicated in Figure 2, a positive trend in the SAM can be observed over the past 40 years. This trend must be caused by positive trends at midlatitudes and/or by negative trends in subpolar latitudes, especially in the case of the latitude-based SAM. Figure 3c shows the 500 hPa GPH trend of ERA-Interim data characterized by a significant positive trend at lower midlatitudes and negative (but insignificant) trends at high midlatitudes and polar latitudes for the reference period 1981–2010. A similar but stronger and more significant, trend pattern was also found in the NCEP/NCAR data set (Figure 3d). Here, however, a widespread and strong positive trend in the 500 hPa GPH over the Antarctic continent is detected, which is indicated in only a small and insignificant region over East Antarctica in the ERA-Interim data set. The trend pattern of the JRA-55 500 hPa level shows positive trends at midlatitudes and polar latitudes but almost no (and therefore insignificant) negative trend at subpolar latitudes. By comparing the three trend patterns, the relatively high correlations for the cumulative SAM time series can be explained. ERA-Interim shows a positive trend both in midlatitudes and a negative trend in polar latitudes. This trend is captured by both the PCA-based and the latitude-based SAM approaches. The additional positive trends for NCEP/NCAR and JRA-55 in high polar latitudes cancel out this generally increasing gradient between midlatitudes and polar latitudes, and no significant correlations were found for the cumulative SAM time series. Owing to the strong agreement between the PCA/ERA-Interim-based SAM approach, NOAA/CPC's SAM, and the latitude-based approach for the three reanalysis, further results in this study refer to the PCA-based SAM method in combination with the ERA-Interim data set. Furthermore, other studies have demonstrated the strong model performance of ERA-Interim in polar latitudes of the SH (Bracegirdle, 2013; Bracegirdle & Marshall, 2012).

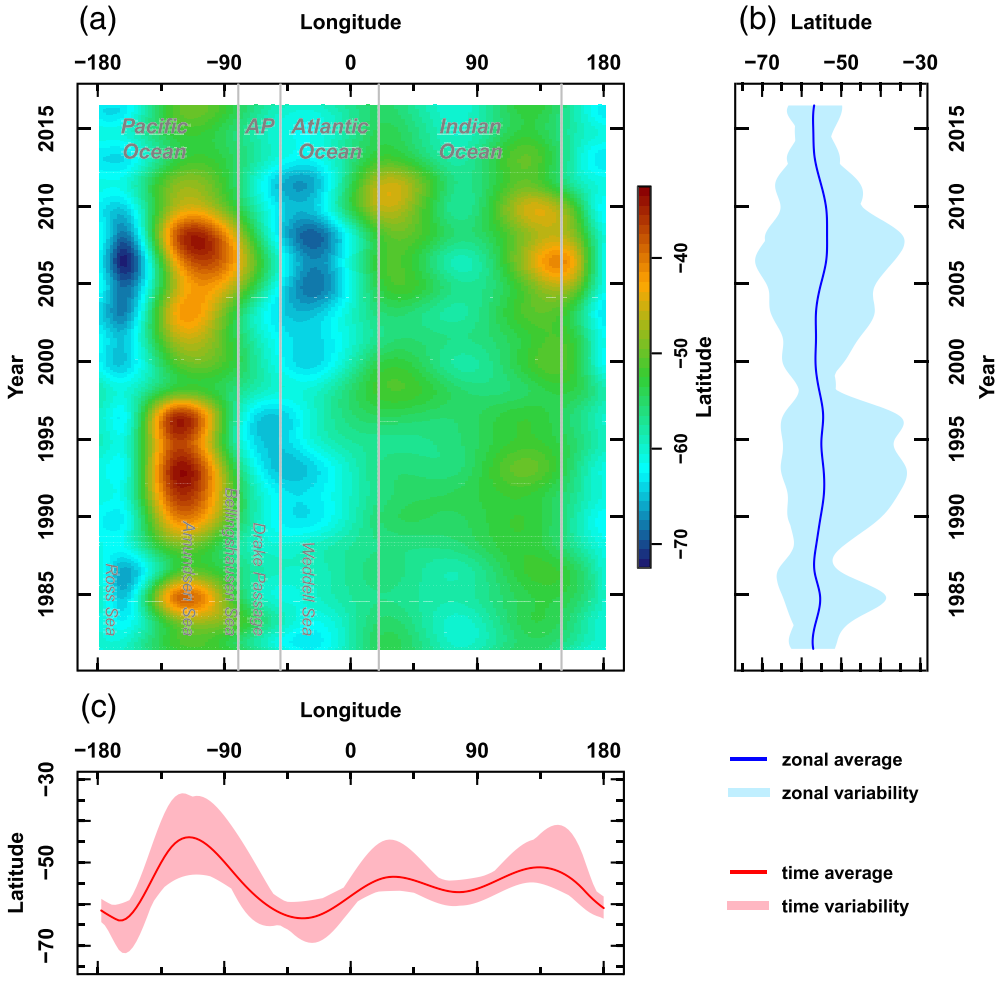

Figure 4. (a) Hovmöller diagram showing the latitudinal positions of the SAM structure dependent on geographic longitude and time; (b) zonally averaged latitude position of the SAM structure and its minimum and maximum extent over time; and (c) averaged SAM structure positions over time and their minimum and maximum extents along longitudes.

3. Results

3.1. Spatiotemporal SAM Pattern Variability

In section 2.2, the main feature of the SAM pattern was described as the transposition zone between regions of positive and negative covariances. The result of the automated mapping of this zone, hereafter, called SAM structure, for the period 1979–2018 is shown in Figure 4. According to the regression period length of 60 months, the time records in Figure 4 refer to the period from July 1981 to June 2016. The Hovmöller diagram (Figure 4a) displays the latitudinal SAM structure positions dependent on the geographic longitude and time. Figure 4b shows the zonal variability over all longitudes over time, whereas Figure 4c indicates the latitudinal SAM structure variability for all longitudes over time. With this evaluation, it can be demonstrated that the SAM structure exhibits large variations over time and deviates significantly from a circumpolar and annular structure. As Figure 4a in combination with Figure 4c shows, the most dominant northward located part of the SAM structure is found in the western hemisphere located around the Amundsen Sea low (Fogt et al., 2011; Scott et al., 2019). In the Ross Sea and Weddell Sea, we find the most southern positions of the SAM structure. Two minor, but still significant, regions of latitudinal variability are located between 0° and 45°E as well as between 120°E and 170°E along the East Antarctic coast. In particular, the minimum and maximum center positions of the SAM structure vary by a few tens of degrees in

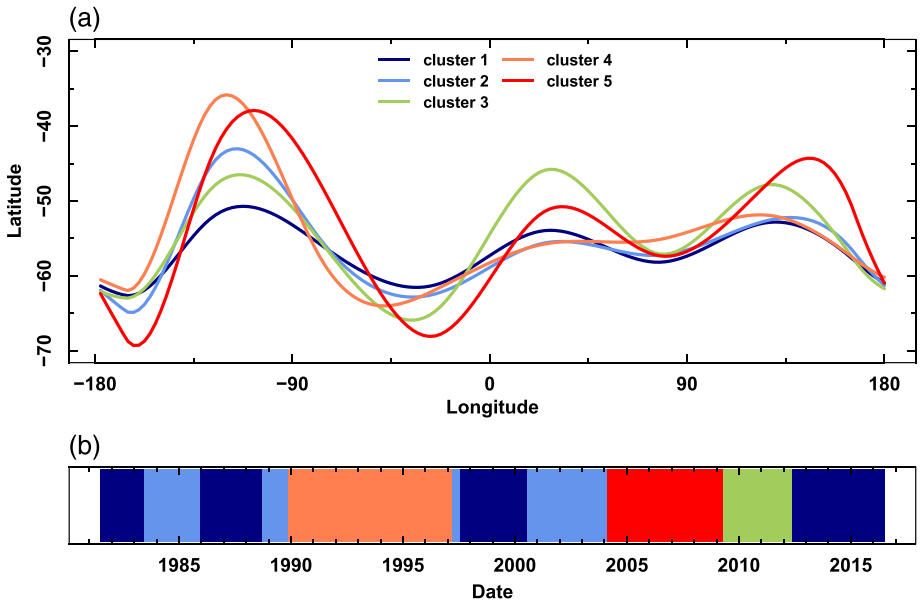

Figure 5. (a) Five different modes of the SAM structure derived from a K-means cluster analysis of the data set shown in Figure 4a; (b) indicates the sections between 1981 and 2016 when the respective clusters were present.

longitude, which indicates remarkable zonal shifts during the investigation period. Figure 4b indicates different phases when the SAM structure was annularly arranged around Antarctica for relatively short periods around 1982, 1987, 1998–1999, and 2015. Periods of large latitudinal variability were found in 1985, 1990–1997, and 2002–2010.

The Hovmöller diagrams of different seasons are presented in Appendix A. As these additional figures and further explanations would exceed the scope of the main part of this paper, the most important characteristics and temporal matches with SH Ozone hole anomalies are briefly mentioned in Appendix A.

3.2. Atmospheric Circulation and Temperature Composites

To quantitatively categorize and temporally locate different SAM structure modes (hereafter called clusters), a k-means cluster analysis (Hartigan & Wong, 1979) was applied to the SAM structure data set, as shown in Figure 4a. Here, we used the results for five different clusters (Figure 5a), which explain 77% of the entire SAM structure variability and have been determined according to the elbow method. Cluster 1 describes the most annular SAM structure, and Cluster 2 represents an increased meridional component in the Amundsen Sea region. A dominant zonal wave-three pattern is indicated by Cluster 3, whereas Clusters 4 and 5 describe a northward shifted SAM structure in the Amundsen Sea region. Cluster 4 shows a slightly eastward shifted maximum, and Cluster 5 represents a westward shifted maximum with most southern positions in the Ross Sea and Weddell Sea. Figure 5b indicates the period when the respective clusters were present. Clusters 1 and 2 reoccurred over the entire investigation period, whereas Cluster 3 was only present between 2009 and 2012, Cluster 4 dominated the years 1990–1996, and Cluster 5 was present between 2004 and 2008.

The varying presence of different clusters was investigated in more detail by calculating atmospheric circulation composites for the respective time sections indicated in Figure 5b. Here, the 500 hPa GPH anomaly composites and the 10 m wind field data were employed to synoptically interpret Antarctic station temperature anomalies. Significant regions of the GPH anomaly ($p < 0.05$) were identified using the Wilcoxon test and are indicated as dotted regions in Figures 6–8. The mean temperature anomalies of samples according to the respective cluster composites were tested for significant deviations from zero using the Wilcoxon test. Figure 6 shows the composites for GPH anomalies (panels a and b), 10 m wind anomalies (panels c and d), and temperature anomalies for Antarctic stations (panels e and f), as introduced in Figure 1, section 2.1.

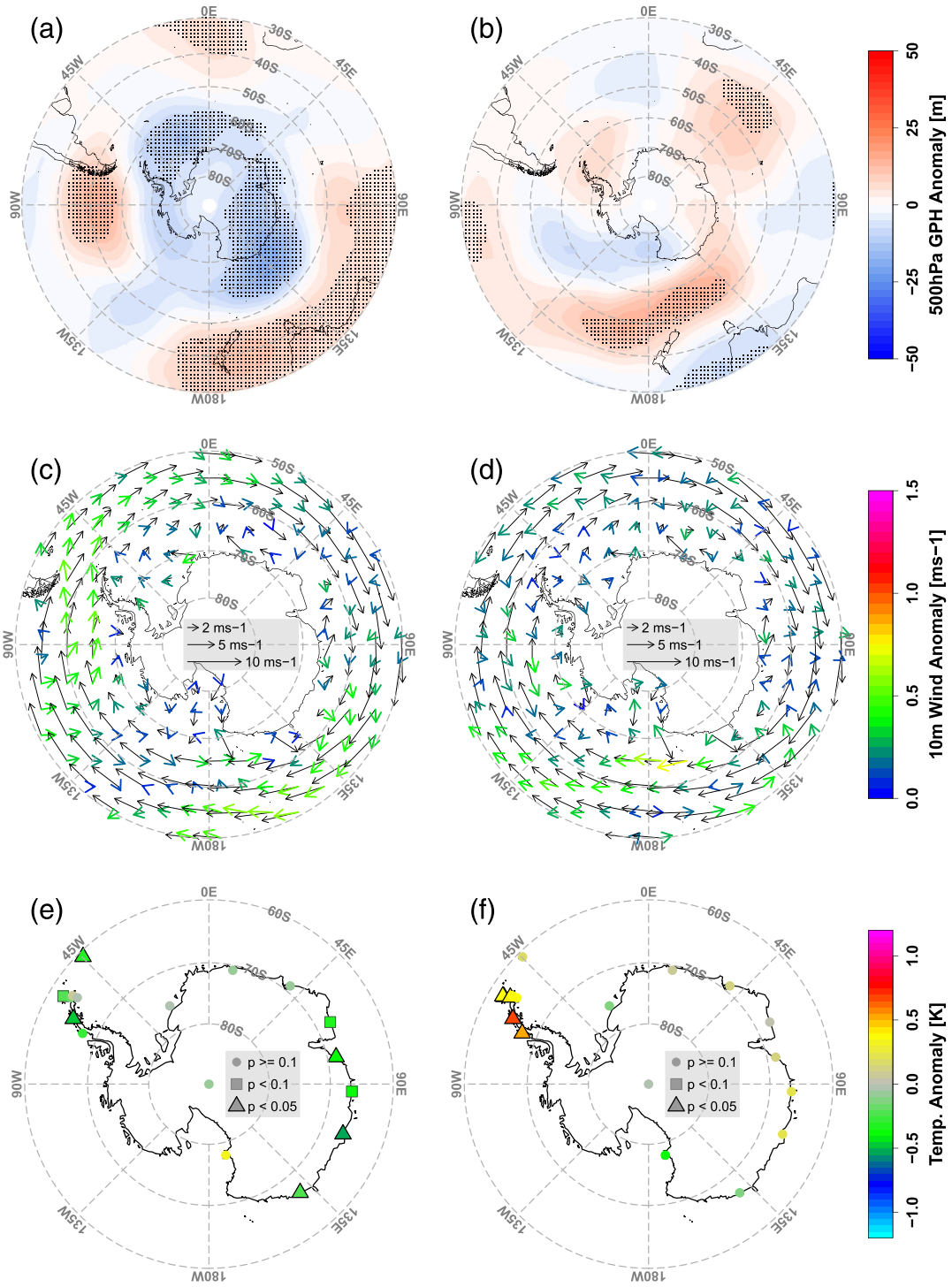

Figure 6. Composites for ERA-Interim 500 hPa GPH anomalies (a and b), ERA-Interim 10 m wind (c and d), and CRUTEM4 Antarctic station temperature anomalies (e and f) for Cluster 1 (a, c, and e) and Cluster 2 (b, d, and f). Black wind vectors in (c) and (d) indicate the long-term average wind field for the reference period 1981–2010. GPH anomaly significances are based on the Wilcoxon test (dotted areas, $p < 0.05$), temperature anomaly significances were determined using the Wilcoxon test, and their significance levels are indicated by different point symbols.

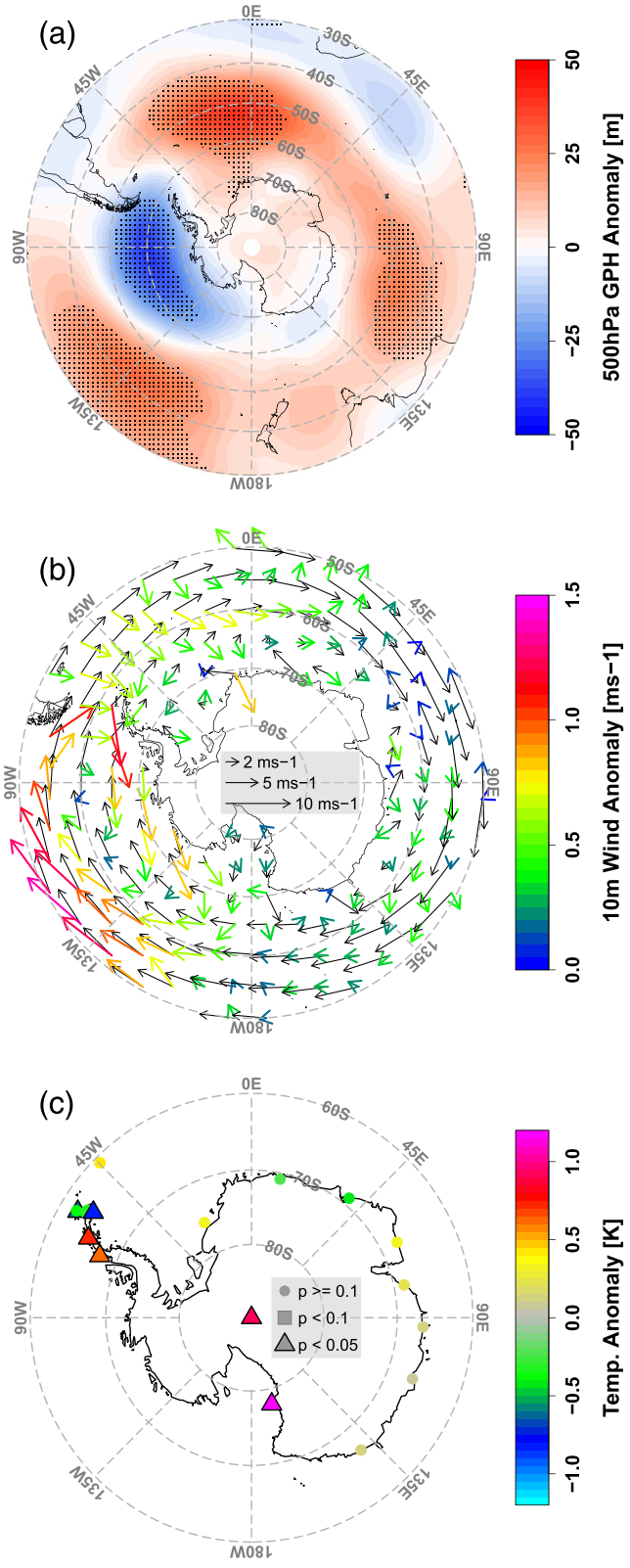

Figure 7. Like Figure 6 but for the Cluster 3.

Although the composites correspond to the time periods of different SAM structure clusters, the anomaly patterns of the circulation may show significant deviations from the "traditional" SAM pattern (Figure 2). The temporary occurrence of other circulation modes can be expected, since the SAM is considered to be the dominant, but not the exclusive circulation mode of the SH.

Figures 6a, 6c, and 6e refer to Cluster 1, and Figures 6b, 6d, and 6f show the composites of Cluster 2. Cluster 1 is characterized by a zonally structured SAM pattern. The GPH composite shows negative GPH anomalies over the polar latitudes and high-pressure anomalies over Australia and New Zealand, as well as over the southeastern Pacific. In particular, the southeastern Pacific anomaly caused a circulation anomaly over the Amundsen and Bellingshausen Seas, which led to the advection of polar air masses toward the Antarctic Peninsula, which is indicated by an increased southwesterly wind anomaly component over the Bellingshausen Sea (Figure 6c). According to this enhanced advection of cold air, temperatures are significantly lower around the Antarctic Peninsula when Cluster 1 is predominant. For East Antarctic stations between 45°E and 135°E, we also found negative temperature anomalies that were presumably caused by an increased advection of cold continental air. This advection could be related to increased cyclonic activity indicated by low-pressure anomalies over the East Antarctic continent. Cluster 2 represents a weak zonal wave-three anomaly pattern around the Antarctic continent, with an increased meridional circulation component in the Pacific sector. The GPH composite (Figure 6b) shows no particularly significant anomalies over the Antarctic continent. A wave train system is found in the Pacific sector, indicated by alternating but insignificant high- and low-pressure anomalies extending from the east Pacific across the Ross, Amundsen, and Bellingshausen Seas to the south Atlantic. The negative GPH anomaly over the northern Amundsen Sea might have triggered intrusions of maritime Pacific air, which is indicated by north- to northeasterly wind anomalies around 90°W. In combination with the predominant westerly winds, this maritime air is transported toward the Antarctic Peninsula and results in temperatures significantly above normal at Antarctic Peninsula stations. Temperature anomalies around East Antarctic stations show no significant deviations from zero.

The composites of Cluster 3 represent a PSA1 circulation anomaly pattern. The 500 hPa GPH anomaly field is characterized by significant high-pressure anomalies over the Pacific, Atlantic, and Indian Oceans. This composite also reveals a significant low-pressure anomaly reaching from the northern Amundsen Sea, across the Bellingshausen Sea, and into the Drake Passage between South America and the Antarctic Peninsula. Corresponding with this distinct GPH anomaly pattern, we found a 10 m wind anomaly pattern as well as significant temperature anomalies at the Antarctic Peninsula, at the South Pole station, and at McMurdo. Although the temperature anomaly signals on the Antarctic Peninsula have different signs (negative at the northern Antarctic Peninsula and positive at the southern Antarctic Peninsula), they can be explained by atmospheric circulation. Owing to the low-pressure and wind anomalies in the western Drake Passage, air masses are advected from the north or northeast. In combination with the high-pressure anomaly over the northeastern Weddell Sea, we found a considerable easterly wind anomaly, east of the Antarctic Peninsula. Thus, the relative warm air

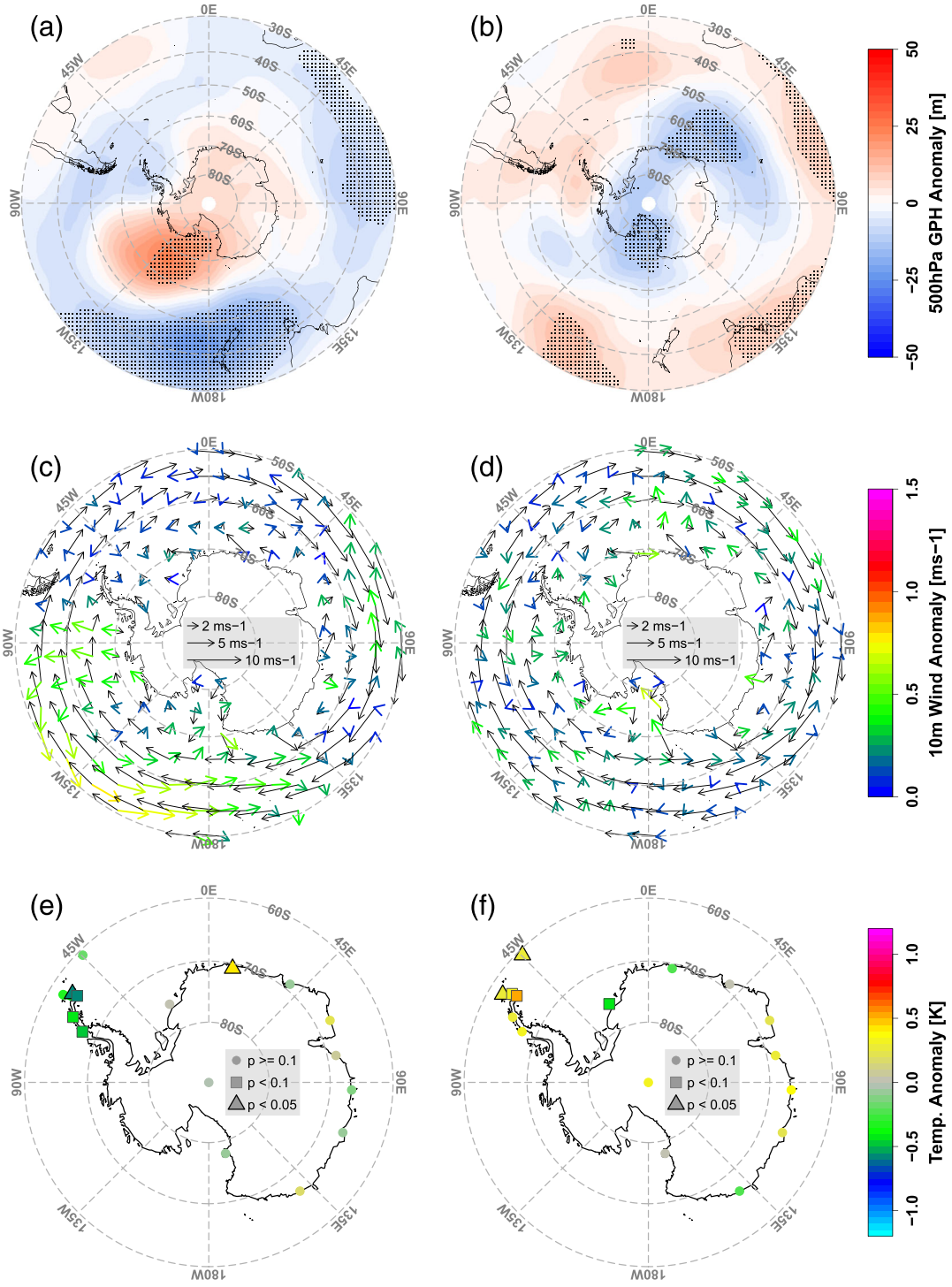

Figure 8. Like Figure 6 but for the Clusters 4 and 5.

associated with the low-pressure anomaly and cold air masses from the Weddell Sea could blend and be transported toward the northern Antarctic Peninsula. According to the negative temperature anomalies at the northern Antarctic Peninsula, the advection of cold Weddell Sea air masses was presumably more effective and caused this northern Antarctic Peninsula cooling period. The positive temperature anomalies at Faraday/Vernadsky and Rothera can be related to the predominant advection of air from the

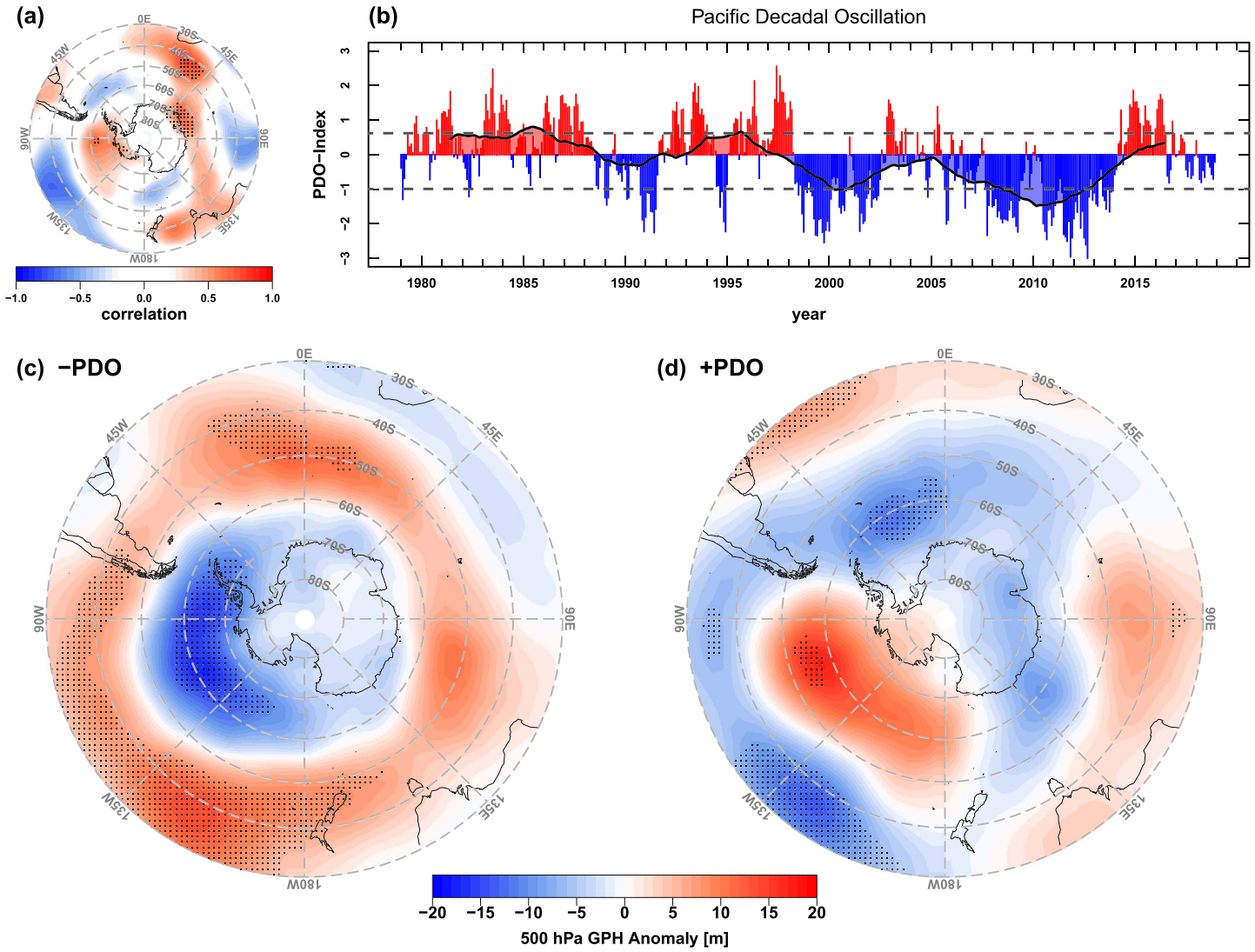

Figure 9. (a) Partial correlation between the SAM pattern data set and the 60 months running mean Pacific Decadal Oscillation (PDO) time series shown as black solid line in (b). Regions of significant correlation are indicated with black dots ($p < 0.1$, considering autocorrelation). Gray dashed lines in (b) indicate lower and upper quartiles, which define phases of positive and negative PDO. The 500 hPa GPH anomaly composites for negative (−PDO, below lower quartile) and positive (+PDO, above upper quartile) phases of PDO are shown in (c) and (d). Significant 500 hPa GPH anomaly regions (dotted areas in c and d) are based on the Wilcoxon test ($p < 0.05$).

north to the south, which leads to positive anomalies at middle and southern Antarctic Peninsula stations. Furthermore, the significant low-pressure anomaly over the Amundsen and Bellingshausen Seas forced the cyclonic advection of warm air from the northern Weddell Sea toward the Antarctic interior and the South Pole (see the 10 m wind anomaly pattern between 45°W and 0°). This warming mechanism for the South Pole was also documented by Clem et al. (2020), who assigned this Pacific wave train pattern to SST anomalies in the western tropical Pacific. They showed that the strongest South Pole warming event occurred from 1997 to 2018. Our Cluster 3 period from 2009 to 2012 coincides with their study period and is probably the period of the strongest South Pole warming. A further correspondence with the results presented here is found in the study by Turner et al. (2016), who reported an absence of further warming and even a cooling trend in the Antarctic Peninsula area since 1999. They also relate these negative temperature anomalies to a significant pressure anomaly over the Drake Passage with the advection of cold Weddell Sea air masses from the east toward the northern Antarctic Peninsula. Our Clusters 1 and 3

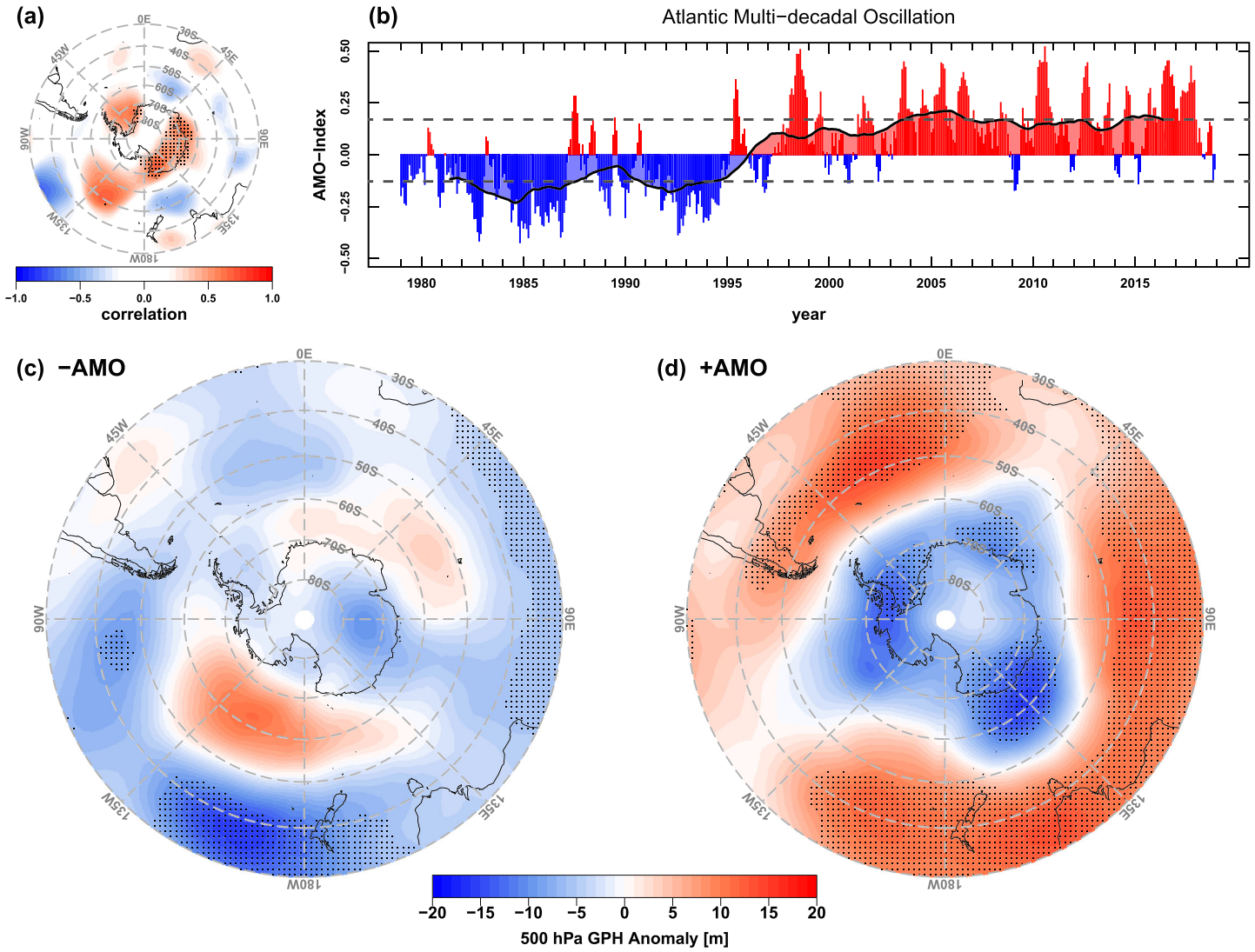

Figure 10. (a) Partial correlation between the SAM pattern data set and the 60 months running mean Atlantic Multidecadal Oscillation (AMO) time series shown as black solid line in (b). Regions of significant correlation are indicated with black dots ($p < 0.1$, considering autocorrelation). Gray dashed lines in (b) indicate lower and upper quartiles, which define phases of positive and negative AMO. The 500 hPa GPH anomaly composites for negative (−AMO, below lower quartile) and positive (+AMO, above upper quartile) phases of AMO are shown in (c) and (d). Significant 500 hPa GPH anomaly regions (dotted areas in c and d) are based on the Wilcoxon test ($p < 0.05$).

are predominant since 2009, and both clusters are related to negative temperature anomaly composites. Thus, the temporal occurrences of Clusters 1 and 3 are in strong agreement with the temperature decrease at Antarctic Peninsula stations discussed by Turner et al. (2016).

In Figure 8, composites for Cluster 4 (panels a, c, and e) and Cluster 5 (panels b, d, and f) are shown. Cluster 4, characterized by a northeastward shifted SAM structure in the Amundsen Sea, reveals a strong high-pressure anomaly over the eastern Ross and western Amundsen Seas. Associated with this strong high-pressure anomaly, we found a northward directed air flow from the West Antarctic continent into the Bellingshausen Sea, which causes, in combination with the circumpolar westerlies, significantly negative temperatures at Antarctic Peninsula stations. The moderately positive temperature anomaly at Novolazarevskaya Station cannot be explained from the large-scale circulation, and all other stations show no significant temperature anomaly. Composites of Cluster 5, which were predominant during the Years 2004–2008, show significantly positive temperature anomalies for the northern Antarctic Peninsula

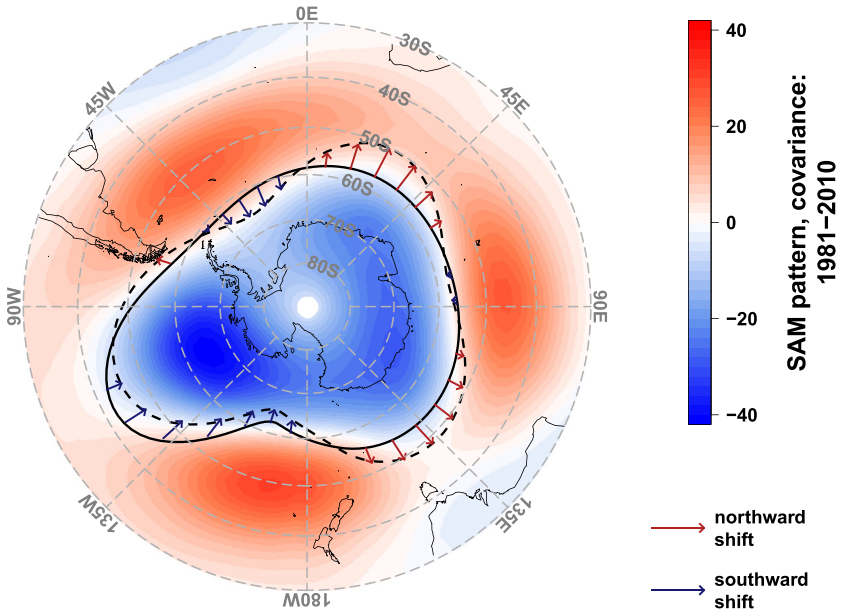

Figure 11. Spatial trend of the SAM structure pattern between 1981 (solid line) and 2016 (dashed line), estimated by linear trends calculated along longitudinal sectors of 10° of the data set shown in Figure 4a.

stations. The positive Antarctic Peninsula temperature anomalies might be related to a low-pressure anomaly over the northern Amundsen Sea between 50–60°S and 100–120°W, where northerly wind anomalies can be found along 90°W. This wind anomaly might have caused an advection of warmer air masses into the Amundsen and Bellingshausen Seas. Thus, the origin of air masses transported with the westerly winds toward the Antarctic Peninsula was more influenced by midlatitude maritime air than by Antarctic air masses, which might have caused above normal temperatures. At East Antarctic stations, the significant low-pressure anomaly over the western Indian Ocean advected oceanic air toward the Antarctic continent, which caused above normal temperatures at stations between 45°E and 135°E.

3.3. Pacific and Atlantic Teleconnections With SAM Pattern Variability

We used the PDO and AMO time series from 1979 to 2018 to examine internal climate influences on the SAM pattern variability on multiannual to decadal time scales. As the studies by Clem and Fogt (2015), Turner et al. (2016), and Clem et al. (2020) demonstrated, significant correlations can be found between the tropical Pacific and Antarctic climate. Furthermore, Li et al. (2014) and Li et al. (2015) studied Rossby wave train coupling between the tropical Atlantic and West Antarctica. In Figures 9 and 10, we examine the correlation between the SAM pattern variability and the temporally congruent 60 months running mean PDO and AMO time series. To investigate the correlation between PDO, AMO, and SAM pattern variability statistically separated, we derived the partial correlation pattern for PDO and SAM pattern (excluding the AMO-SAM pattern correlation) shown in Figure 9a. The partial correlation between AMO and SAM pattern variability is shown in Figure 10a.

Both correlation patterns (Figures 9a and 10a) reveal significant correlations with circum-Antarctic wave train patterns of different signs for SAM pattern variability and the PDO and AMO indices, respectively. For the PDO-SAM pattern correlation, we find a zonal wave-two pattern south of 50°S and a zonal wave-three pattern for the AMO-SAM pattern correlation. We interpret these teleconnection patterns as an indicator of the ocean-induced influence on atmospheric circulation variability around Antarctica. For the first half of the study period, PDO was in its positive phase (cool North Pacific SST) and AMO in the negative phase (cool north Atlantic SST). The 500 hPa composites for both indices reveal positive GPH anomalies over the southern Pacific Ocean (Figures 9d and 10c). Such a positive anomaly was also found for Cluster 4 (Figure 8a). This cluster was present from 1990 to 1997, which coincides with years of positive PDO and negative AMO conditions. During the negative PDO phase (warm central North Pacific SST), which

mainly refers to the period since the late 1990s, we found a significantly deeper Amundsen and Bellingshausen Seas low (Figure 9c). Cluster 3 also revealed such a GPH anomaly and was identified to drive positive temperature anomalies over the Antarctic interior. This negative GPH anomaly over the Amundsen and Bellingshausen Seas in combination with the high-pressure anomaly over the Pacific (30–45°S) can be related to the southward trend of the SAM pattern in the central Pacific, as indicated in Figure 11 by the blue arrows. The composite of the positive AMO (positive sea SST anomalies in the north Atlantic), predominantly since the mid-1990s, is related to negative 500 hPa GPH anomalies over East Antarctica, centered around 45°E and 135°E. These regional pressure anomalies caused a northward trend of the SAM pattern, as indicated by the red arrows in Figure 11. The seasonal analysis of the SAM structure in Appendix A (Figure A4) also shows a northward displacement of the SAM structure in JJA around the Year 2015 between 0° and 45°E. Thus, this northward trend can mainly be associated with changes in the SAM pattern during winter. The southward directed SAM pattern trend in the Atlantic sector is tied to the positive pressure anomaly between 45°W and 0°. This south Atlantic trend pattern is most likely related to the austral autumn and winter months as the seasonal SAM structure analysis in Figures A3 and A4 indicate southward displacements in the Weddell Sea sector since 1995 (in MAM) and 2000 (in JJA). The linear trend estimates for spatial shifts of the SAM structure between 1981 and 2016 for the 10° longitudinal sectors were calculated on the basis of the data set presented in Figure 4a. The SAM loading pattern in Figure 11 refers to the reference period 1981–2010, and it is similar to the pattern shown in Figure 2.

4. Summary and Conclusions

The present study has demonstrated that the SAM and its annularity structure varied significantly during the past four decades. We introduced the cumulative SAM analysis, which was used to highlight seasonal to multiannual accumulations of positive or negative SAM index values. Furthermore, this statistical assessment served as a sensitive measure for comparing different SAM time series, which depend on different reanalysis data sets and were derived by three different analysis approaches. With the strongest performance found using the PCA-based/ERA-Interim SAM, we derived a spatiotemporally resolved SAM pattern data set that was analyzed with respect to the SAM pattern structure. The systematic long-term analysis of the SAM structure on multiseasonal to decadal time scales is a novel approach and contributes new insights into the varying shape of the SAM annularity. With the categorization of different clusters, we found atmospheric patterns that were used to synoptically explain station temperature anomalies around the Antarctic continent by SH circulation anomaly patterns. Most frequently, significant temperature anomalies were found at Antarctic Peninsula stations, depending on the respective cluster (Figures 6–8). This is especially due to intense pressure anomalies in the south Pacific and in the area of the Amundsen and Bellingshausen Seas low. This area of maximum SAM structure variability (see Figure 4) can therefore be regarded as an important region of circulation variability that subsequently affects the temperature variability at the Antarctic Peninsula.

Strong correlations between the SAM pattern variability and oceanic SST anomalies in the northern Atlantic and northern Pacific, represented by AMO and PDO, indicated interhemispheric teleconnection patterns. Such couplings by SST induced Rossby wave trains have been reported in other studies (Clem et al., 2020; Li et al., 2014, 2015; Turner et al., 2016). In the Pacific sector, the influence of PDO, especially on the Amundsen and Bellingshausen Seas low, and thus on the Pacific pattern variability of SAM, is predominant. In the south Atlantic and in areas of the East Antarctic, spatial trends in the SAM pattern were related to GPH anomalies, which are significantly correlated with the positive AMO phase. Since 1979, the signs of PDO and AMO have reversed from a cooler (+PDO, −AMO) to a warmer phase (−PDO, +AMO) at about the same time in the middle/late 1990s. The associated GPH anomalies of SH could explain spatial trends in the SAM pattern. Furthermore, the intensification of the pressure gradient between midlatitudes and polar latitudes, shown in Figures 9c and 10d, could also explain the positive trend of the SAM in recent decades. Owing to the significantly different periodicities of PDO (15–25 years; Mantua & Hare, 2002) and AMO (60–75 years; Schlesinger & Ramankutty, 1994), a non-uniform change in these important climate parameters occurred for the first time during the modern satellite era since 1979. In 2014, the PDO changed its signal from negative to positive phase. Therefore, it might be of interest for future work on SH climate variability to consider the possible influences of PDO and AMO and their different signs.

Appendix A: Seasonal SAM Structure Variability

Seasonal evaluations of SAM structure variability (Hovmöller diagrams) are presented in this appendix. They were prepared using the same methodology as described in section 3.1 and shown in Figure 4. To show possible temporal correlations with the ozone hole, which is an important component in the SH climate system, data of the Ozone hole extent were added for the austral spring and summer season (source: Ozone watch, NASA).

As described in other studies before (e.g., Fogt, Jones, et al, 2012), we also find the most annular SAM structure in DJF (Figure A2) and the largest meridional variability in JJA (Figure A3). Although the methodology used here was not primarily developed to investigate the relationship between ozone and the SH circulation, we also found temporal matches between the extent of the ozone hole and our SAM structure variability. Between 1979 and 1985, when the area of the ozone hole was small, the zonal SAM structure during DJF was predominantly zonal with only low latitudinal variability (Figure A2b). Another interesting period with a reduced zonal SAM structure variability can be found around the Year 2002 during SON (Figure A1). In 2002, the small extent of the ozone hole (associated with a sudden stratospheric warming event and split of the polar vortex; Hio & Yoden, 2005) coincides with a more annular SAM pattern structure. Due to the applied regression approach over 5 years (60 months), such events on monthly to seasonal time scales could only be detected very imprecisely. Nevertheless, these first insights can serve as motivation to further develop the analysis approach for studies on seasonal time scales.

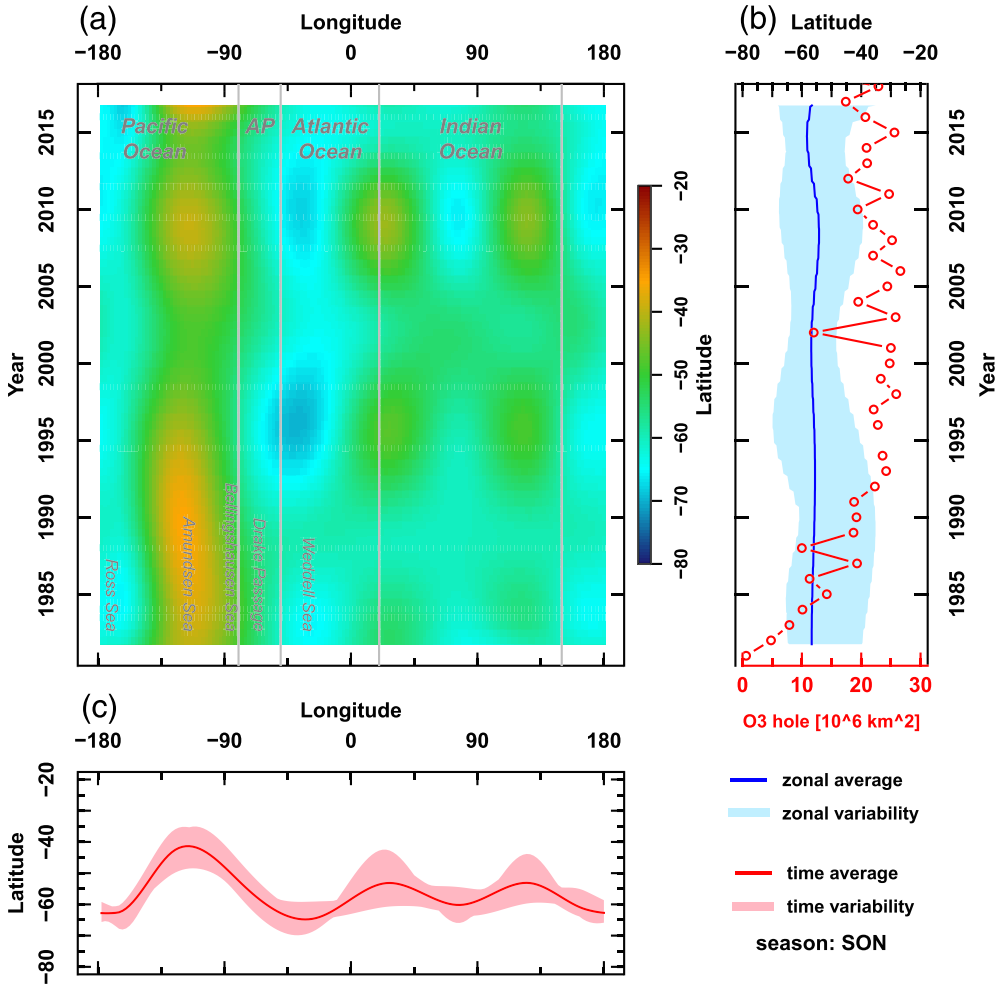

Figure A1. (a) Hovmöller diagram showing the latitudinal positions of the SAM structure dependent on geographic longitude and time for SON; (b) zonally averaged latitude position of the SAM structure in SON and its minimum and maximum extent over time; and (c) averaged SAM structure positions over time and their minimum and maximum extents along longitudes in SON.

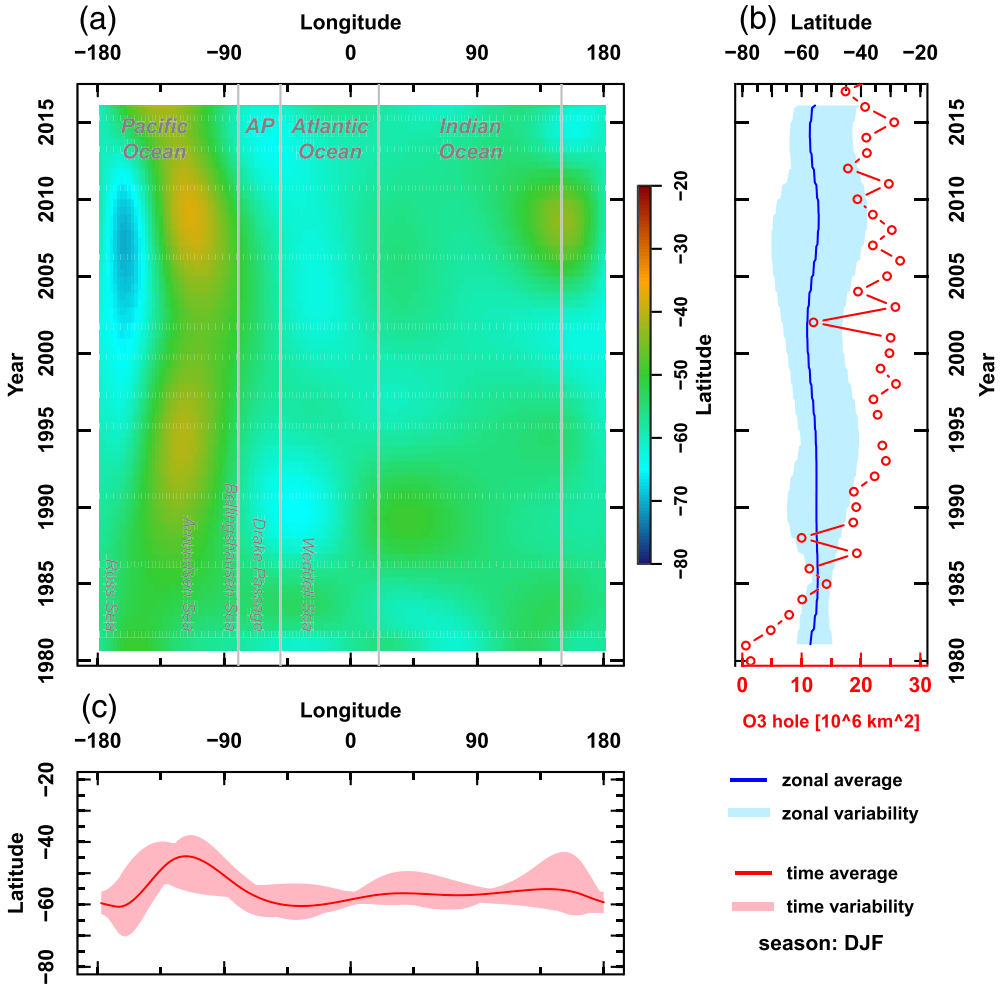

Figure A2. Same analysis like Figure A.1 but for austral summer (DJF).

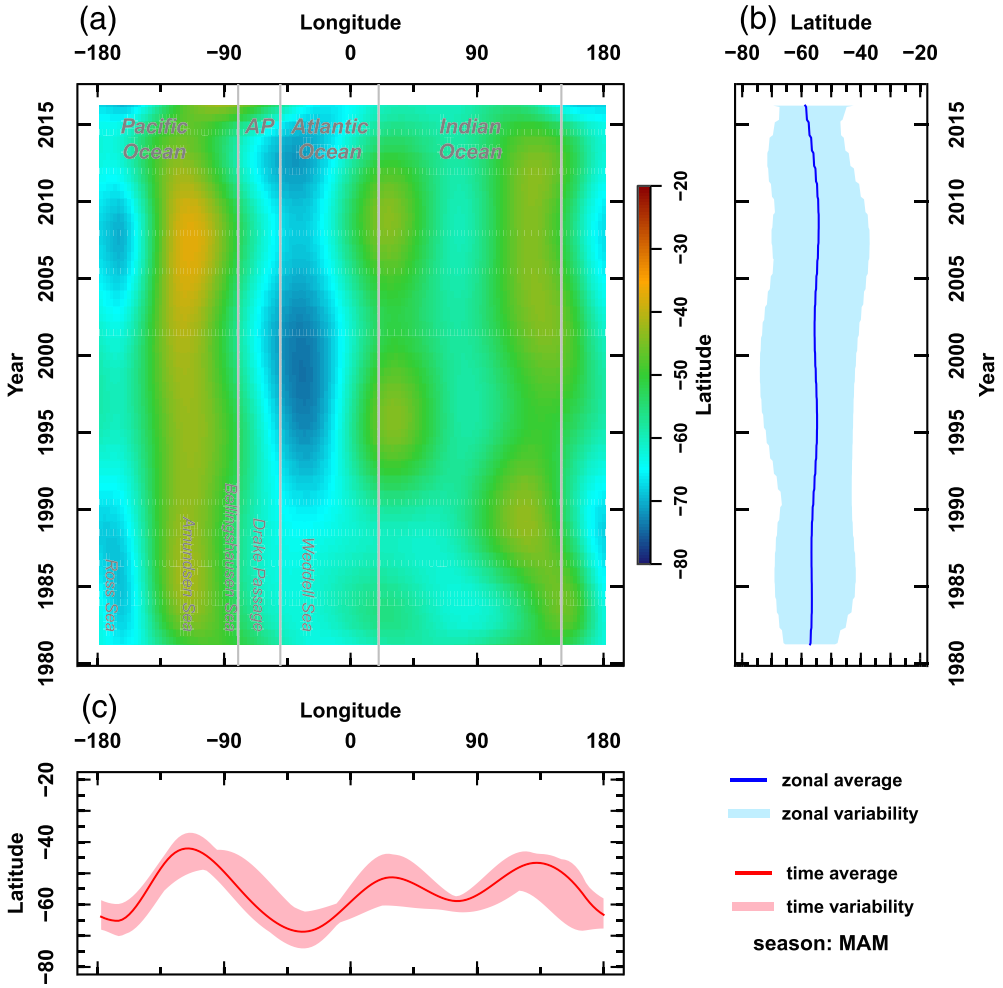

Figure A3. Same analysis like Figure A.1 but for austral autumn (MAM).

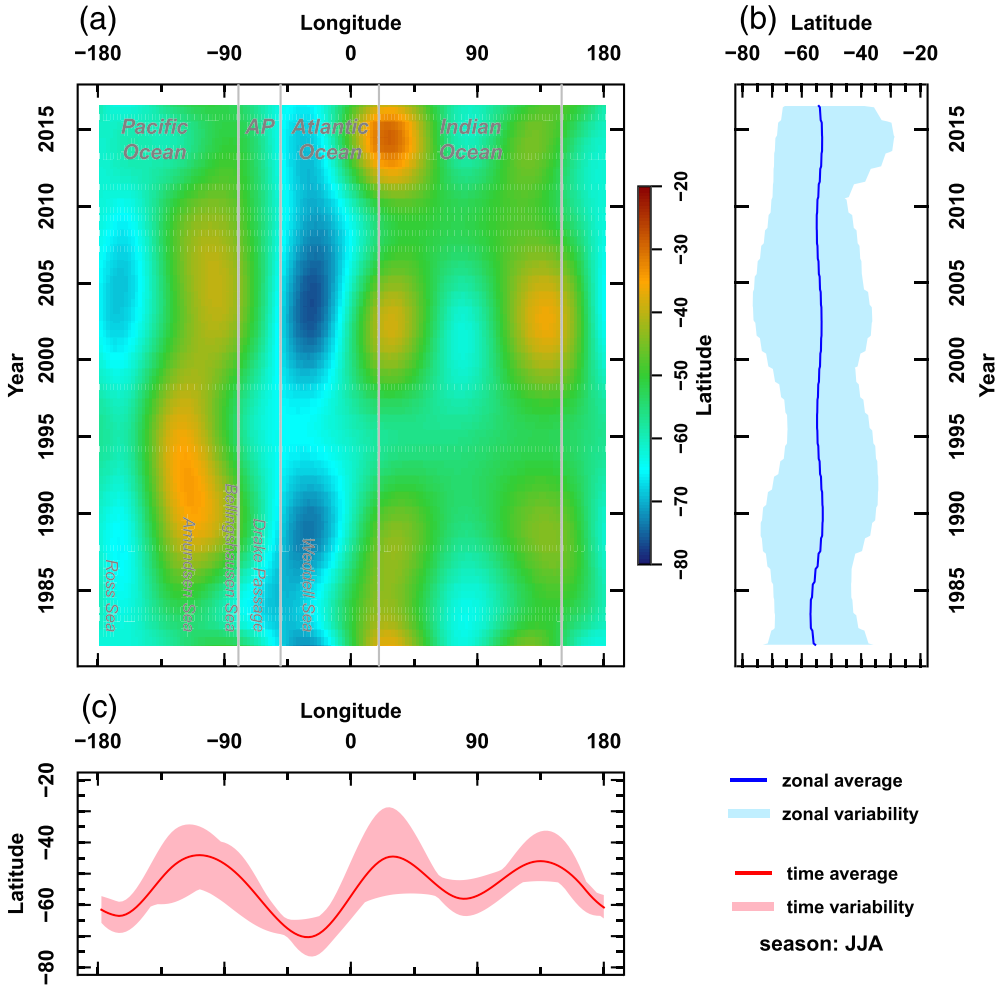

Figure A4. Same analysis like Figure A.1 but for austral winter (MAM).

Data Availability Statement

All data used in this work are freely available: ERA-Interim reanalysis, European Centre for Medium-Range Weather Forecasts (https://www.ecmwf.int/en/forecasts/datasets/reanalysis-datasets/era-interim); NCEP/NCAR reanalysis, National Center for Atmospheric Research of the National Centers for Environmental Predictions (https://psl.noaa.gov/data/reanalysis/reanalysis.shtml); JRA-55 reanalysis, Climate Prediction Division of the Japan Meteorological Agency (https://jra.kishou.go.jp/JRA-55/index_en.html); CRUTEM4 station temperature data, Met Office Hadley Centre, and the Climatic Research Unit at the University of East Anglia (https://www.metoffice.gov.uk/hadobs/crutem4/data/download.html); G. Marshall, SAM data (https://legacy.bas.ac.uk/met/gjma/sam.html); NOAA/CPC, SAM data (https://www.cpc.ncep.noaa.gov/); PDO index, NOAA's National Centers for Environmental Information (https://www.ncdc.noaa.gov/teleconnections/pdo/); AMO data, NOAA's Physics Science Laboratory (PSL, https://psl.noaa.gov/data/correlation/amon.us.data); and Ozone hole extent (in Appendix A), Ozone Watch of the National Aeronautics and Space Administration (NASA, https://ozonewatch.gsfc.nasa.gov/statistics/annual_data.html).

Acknowledgments

The authors would like to gratefully acknowledge the financial support and endorsement from the DLR Management Board Young Investigator Group Leader Program. We would also like to thank the three anonymous reviewers for their valuable feedback. Open access funding enabled and organized by Projekt DEAL.

References

Arblaster, J. M., & Meehl, G. (2006). Contributions of external forcings to Southern Annular Mode trends. *Journal of Climate*, *19*(12), 2896–2905. https://doi.org/10.1175/JCLI3774.1

Bracegirdle, T. J. (2013). Climatology and recent increase of westerly winds over the Amundsen Sea derived from six reanalyses. *International Journal of Climatology*, *33*(4), 843–851. https://doi.org/10.1002/joc.3473

Bracegirdle, T. J., & Marshall, G. J. (2012). The reliability of Antarctic tropospheric pressure and temperature in the latest global reanalyses. *Journal of Climate*, *25*, 7138–7146. https://doi.org/10.1175/JCLI-D-11-00685.1

Clem, K. R., & Fogt, R. L. (2015). South Pacific circulation changes and their connection to the tropics and regional Antarctic warming in austral spring, 1979–2012. *Journal of Geophysical Research: Atmospheres*, *120*, 2773–2792. https://doi.org/10.1002/2014JD022940

Clem, K. R., Fogt, R. L., Turner, J., Lintner, B. R., Marshall, G. J., Miller, J. R., & Renwick, J. A. (2020). Record warming at the South Pole during the past three decades. *Nature Climate Change*, *10*(8), 762–770. https://doi.org/10.1038/s41558-020-0815-z

Clem, K. R., Renwick, J. A., & McGregor, J. (2016). Relationship between eastern tropical Pacific cooling and recent trends in the Southern Hemisphere zonal-mean circulation. *Climate Dynamics*, *49*(1–2), 113–129. https://doi.org/10.1007/s00382-016-3329-7

Clem, K. R., Renwick, J. A., McGregor, J., & Fogt, R. L. (2016). The relative influence of ENSO and SAM on Antarctic Peninsula climate. *Journal of Geophysical Research: Atmospheres*, *121*, 9324–9341. https://doi.org/10.1002/2016JD025305

Dee, D. P., Uppala, S. M., Simmons, A. J., Berrisford, P., Poli, P., Kobayashi, S., et al. (2011). The ERA-Interim reanalysis: Configuration and performance of the data assimilation system. *Quarterly Journal of the Royal Meteorological Society*, *137*(656), 553–597. https://doi.org/10.1002/qj.828

Ding, Q., Steig, E. J., Battisti, D. S., & Wallace, J. M. (2012). Influence of the tropics on the Southern Annular Mode. *Journal of Climate*, *25*(18), 6330–6348. https://doi.org/10.1175/JCLI-D-11-00523.1

Enfield, D. B., Mestas-Nunez, A. M., & Trimble, P. J. (2001). The Atlantic Multidecadal Oscillation and its relationship to rainfall and river flows in the continental U.S. *Geophysical Research Letters*, *28*(10), 2077–2080. https://doi.org/10.1029/2000GL012745

Fogt, R. F., Bromwich, D. H., & Hines, K. M. (2011). Understanding the SAM influence on the South Pacific ENSO teleconnection. *Climate Dynamics*, *36*, 1555–1576. https://doi.org/10.1007/s00382-010-0905-0

Fogt, R. L., Jones, J. M., & Renwick, J. (2012). Seasonal zonal asymmetries in the Southern Annular Mode and their impact on regional temperature anomalies. *Journal of Climate*, *25*(18), 6253–6270. https://doi.org/10.1175/JCLI-D-11-00474.1

Fogt, R. L., & Marshall, G. J. (2020). The Southern Annular Mode: Variability, trends, and climate impacts across the Southern Hemisphere. *Wiley Interdisciplinary Reviews: Climate Change*, *11*(4), 1–24. https://doi.org/10.1002/wcc.652

Fogt, R. L., Wovrosh, A. J., Langen, R. A., & Simmonds, I. (2012). The characteristic variability and connection to the underlying synoptic activity of the Amundsen-Bellingshausen Seas Low. *Journal of Geophysical Research*, *117*, D07111. https://doi.org/10.1029/2011JD017337

Garreaud, R. D., & Battisti, D. S. (1999). Interannual (ENSO) and Interdecadal (ENSO-like) variability in the Southern Hemisphere tropospheric circulation. *Journal of Climate*, *12*(7), 2113–2123. https://doi.org/10.1175/1520-0442(1999)012%3C2113:IEAIEL%3E2.0.CO;2

Gong, D., & Wang, S. (1999). Definition of Antarctic oscillation index. *Geophysical Research Letters*, *26*(4), 459–462. https://doi.org/10.1029/1999GL900003

Hartigan, J. A., & Wong, M. A. (1979). A K-means clustering algorithm. *Journal of the Royal Statistical Society: Series C: Applied Statistics*, *28*(1), 100–108. https://doi.org/10.2307/2346830

Hio, Y., & Yoden, S. (2005). Interannual variations of the seasonal march in the Southern Hemisphere stratosphere for 1979–2002 and characterization of the unprecedented year 2002. *Journal of the Atmospheric Sciences*, *62*, 567–580. https://doi.org/10.1175/JAS-3333.1

Ho, M., Kiem, A. S., & Verdon-Kidd, D. C. (2012). The Southern Annular Mode: A comparison of indices. *Hydrology and Earth System Sciences*, *16*, 967–982. https://doi.org/10.5194/hess-16-967-2012

Hosking, J. S., Orr, A., Marshall, G. J., Turner, J., & Phillips, T. (2013). The influence of the Amundsen–Bellingshausen Seas Low on the climate of West Antarctica and its representation in coupled climate model simulations. *Journal of Climate*, *26*(17), 6633–6648. https://doi.org/10.1175/JCLI-D-12-00813.1

Jones, M. J., Fogt, R. L., Widmann, M., Marshall, G. J., Jones, P. D., & Visbeck, M. (2009). Historical SAM variability. Part I: Century-length seasonal reconstructions. *Journal of Climate*, *22*(20), 5319–5345. https://doi.org/10.1175/2009JCLI2785.1

Jones, P. D., Lister, D. H., Osborn, T. J., Harpham, C., Salmon, M., & Morice, C. P. (2012). Hemispheric and large-scale land-surface air temperature variations: An extensive revision and an update to 2010. *Journal of Geophysical Research*, *177*, D05127. https://doi.org/10.1029/2011JD017139

Kalnay, E., Kanamitsu, M., Kistler, R., Collins, W., Deavon, D., Gandin, L., et al. (1996). The NCEP/NCAR 40-year reanalysis project. *Bulletin of the American Meteorological Society*, *77*(3), 437–471. https://doi.org/10.1175/1520-0477(1996)077%3C0437:TNYRP%3E2.0.CO;2

Kayano, M. T., & Setzer, A. W. (2018). Nearly synchronous multidecadal oscillations of surface air temperature in Punta Arenas and the Atlantic Multidecadal Oscillation Index. *Journal of Climate*, *31*(18), 7237–7248. https://doi.org/10.1175/JCLI-D-17-0793.1

Kobayashi, S., Ota, Y., Harada, Y., Ebita, A., Moriya, M., Onoda, H., et al. (2015). The JRA-55 reanalysis: General specifications and basic characteristics. *Journal of the Meteorological Society of Japan. Series II*, *93*(1), 5–48. https://doi.org/10.2151/jmsj.2015-001

Kwok, R., & Comiso, J. C. (2002). Spatial patterns of variability in Antarctic surface temperature: Connections to the Southern Hemisphere Annular Mode and the Southern Oscillation. *Geophysical Research Letters*, *29*(14), 1705. https://doi.org/10.1029/2002GL015415

Li, X., Gerber, E. P., Holland, D. M., & Yoo, C. (2015). A Rossby wave bridge from the tropical Atlantic to West Antarctica. *Journal of Climate*, *28*(6), 2256–2273. https://doi.org/10.1175/JCLI-D-14-00450.1

Li, X., Holland, D. M., Gerber, E. P., & Yoo, C. (2014). Impacts of the north and tropical Atlantic Ocean on the Antarctic Peninsula and sea ice. *Nature*, *505*(7484), 538–542. https://doi.org/10.1038/nature12945

Mantua, N. J., & Hare, S. R. (2002). The Pacific Decadal Oscillation. *Journal of Oceanography*, *58*, 35–44. https://doi.org/10.1023/A:1015820616384

Marshall, G. J. (2003). Trends in the Southern Annular Mode from observations and reanalyses. *Journal of Climate*, *16*(24), 4134–4143. https://doi.org/10.1175/1520-0442(2003)016%3C4134:TITSAM%3E2.0.CO;2

Marshall, G. J. (2007). Half-century seasonal relationships between the Southern Annular Mode and Antarctic temperatures. *International Journal of Climatology*, *27*(3), 373–383. https://doi.org/10.1002/joc.1407

Marshall, G. J., Orr, A., van Lipzig, N. P. M., & King, J. C. (2006). The impact of a changing Southern Hemisphere Annular Mode on Antarctic Peninsula summer temperatures. *Journal of Climate*, *19*(20), 5388–5404. https://doi.org/10.1175/JCLI3844.1

Marshall, G. J., & Thompson, D. W. J. (2016). The signatures of large-scale patterns of atmospheric variability in Antarctic surface temperatures. *Journal of Geophysical Research: Atmospheres*, *121*, 3276–3289. https://doi.org/10.1002/2015JD024665

Nicolas, J. P., Vogelmann, A. M., Scott, R. C., Wilson, A. B., Cadeddu, M. P., Bromwich, D. H., et al. (2017). January 2016 extensive summer melt in West Antarctica favoured by strong El Nino. *Nature Communications*, *8*(1), 1–10. https://doi.org/10.1038/ncomms15799

Previdi, M., & Polvani, L. M. (2014). Climate system response to stratospheric ozone depletion and recovery. *Quarterly Journal of the Royal Meteorological Society*, *140*(685), 2401–2419. https://doi.org/10.1002/qj.2330

Schlesinger, M. E., & Ramankutty, N. (1994). An oscillation in the global climate system of period 65-70 years. *Nature*, *367*, 723–726. https://doi.org/10.1038/367723a0

Scott, R. C., Nicolas, J. P., Bromwich, D. H., Norris, J. R., & Lubin, D. (2019). Meteorological drivers and large-scale climate forcing of West Antarctic surface melt. *Journal of Climate*, *32*(3), 665–684. https://doi.org/10.1175/JCLI-D-18-0233.1

Shindell, D. T., & Schmidt, G. A. (2004). Southern Hemisphere climate response to ozone changes and greenhouse gas increases. *Geophysical Research Letters*, *31*, L18209. https://doi.org/10.1029/2004GL020724

Thompson, D. W. J., & Solomon, S. (2002). Interpretation of recent Southern Hemisphere climate change. *Science*, *296*(5569), 895–899. https://doi.org/10.1126/science.1069270

Thompson, D. W. J., Solomon, S., Kushner, P. J., England, M. H., Grise, K. M., & Karoly, D. J. (2011). Signatures of the Antarctic ozone hole in Southern Hemisphere surface climate change. *Nature Geoscience*, *4*, 741–749. https://doi.org/10.1038/ngeo1296

Thompson, D. W. J., & Wallace, J. M. (2000). Annular modes in the extratropical circulation. Part I: Month-to-month variability. *Journal of Climate*, *13*(5), 1000–1016. https://doi.org/10.1175/1520-0442(2000)013%3C1000:AMITEC%3E2.0.CO;2

Turner, J., Lu, H., White, I., King, J. C., Phillips, T., Hosking, J. S., et al. (2016). Absence of 21st century warming on Antarctic Peninsula consistent with natural variability. *Nature*, *535*(7612), 411–415. https://doi.org/10.1038/nature18645

Van den Broeke, M. R., & van Lipzig, N. P. M. (2004). Changes in Antarctic temperature, wind and precipitation in response to the Antarctic Oscillation. *Annals of Glaciology*, *39*, 119–126. https://doi.org/10.3189/172756404781814654

Visbeck, M. (2009). A station-based Southern Annular Mode Index from 1884 to 2005. *Journal of Climate*, *22*(4), 940–950. https://doi.org/10.1175/2008JCLI2260.1

Wilks, D. S. (2005). Statistical methods in the atmospheric sciences. *International Geophysics Series*, *91*, 627.

Zhang, Y., Wallace, J. M., & Battisti, D. S. (1996). ENSO-like interdecadal variability: 1900–93. *Journal of Climate*, *10*(5), 1004–1020. https://doi.org/10.1175/1520-0442(1997)010%3C1004:ELIV%3E2.0.CO;2